

P. J. Schmid · L. Li · M. P. Juniper · O. Pust

# Applications of the dynamic mode decomposition

Received: 11 May 2009 / Accepted: 5 April 2010 / Published online: 20 August 2010  
© Springer-Verlag 2010

**Abstract** The decomposition of experimental data into dynamic modes using a data-based algorithm is applied to Schlieren snapshots of a helium jet and to time-resolved PIV-measurements of an unforced and harmonically forced jet. The algorithm relies on the reconstruction of a low-dimensional inter-snapshot map from the available flow field data. The spectral decomposition of this map results in an eigenvalue and eigenvector representation (referred to as dynamic modes) of the underlying fluid behavior contained in the processed flow fields. This dynamic mode decomposition allows the breakdown of a fluid process into dynamically relevant and coherent structures and thus aids in the characterization and quantification of physical mechanisms in fluid flow.

**Keywords** Dynamic mode decomposition · Arnoldi method · Iterative techniques · Experimental fluid dynamics

## 1 Introduction

The rise of computational resources and fast algorithms has fueled the detailed analysis of many flow fields. Global stability analyses, i.e., the decomposition of flow fields in complex geometries into modal structures, are becoming increasingly commonplace, and efficient algorithms are available for the extraction of stability information from numerical simulations of flows in complex configurations [22]. In these analyses, the Arnoldi algorithm (and its variations) lies at the center of any computational effort [5]. This algorithm reduces the Jacobian stability matrix by successive orthogonalizations and projections onto an equivalent matrix of smaller size whose eigenvalues approximate some of the eigenvalues of the original system, see [13]. During these procedures the Jacobian matrix or its action on a specific flow field has to be known. This restriction has limited the application of the Arnoldi technique to flow fields from numerical simulations, since only in this case a model (e.g., the linearized and discretized Navier–Stokes equations) is known.

---

Communicated by T. Colonius.

---

P. J. Schmid (✉)  
Laboratoire d'Hydrodynamique (LadHyX), CNRS-Ecole Polytechnique, Palaiseau, France  
E-mail: peter@ladhyx.polytechnique.fr

L. Li · M. P. Juniper  
Department of Engineering, Cambridge University, Cambridge, UK

O. Pust  
Dantec Dynamics, Skovlunde, Copenhagen, Denmark

Experimental data, on the other hand, have been largely processed by data-based algorithms, rather than model-based algorithms. This type of algorithms includes, for example, various statistical techniques, such as mean values, root-mean-square (rms) values, conditional sampling techniques (see, e.g., [1]) or quadrant analyses (see, e.g., [17]). It is however safe to say that in terms of isolating the underlying fluid mechanisms, these statistical techniques are far inferior to the model-based techniques applied to numerically generated data. An exception is given by the proper orthogonal decomposition (POD) technique ([14,2]) which can equally be applied to numerically generated or experimentally measured flow fields [8]. Its premise, however, rests on a hierarchical ranking of coherent structures based on their energy content. Mathematically, it uses an eigenvalue decomposition of a (commonly) time-averaged spatial correlation tensor. The reliance on second-order flow statistics, however, does not *directly* capture the dynamics of the underlying coherent structures and thus limits the information that can be gained about fundamental dominant processes. The decomposition of experimental measurements into temporally and spatially coherent structures is an important tool in the arsenal of any experimentalists, since the breakdown of a flow field into organized, connected and large-scale fluid elements (see [11,21] for examples of a decomposition into coherent structures) allows a more thorough analysis of complex fluid processes.

In this article we introduce and apply a decomposition method, referred to as the dynamic mode decomposition (DMD) [20], that attempts to extract dynamic information from flow fields without relying on the availability of a model, but rather is based on a sequence of snapshots. It thus can be applied equally well to numerically generated flow fields and experimentally measured velocity data. A brief description of the underlying idea of this method will be given (for details the reader is referred to [20]) and various modifications and application possibilities will be listed. Two examples will then demonstrate the potential of this technique: (i) the decomposition of Schlieren snapshots of a helium jet and (ii) the decomposition of time-resolved PIV-measurements of an unforced and forced jet. The two examples have been chosen to showcase how the decomposition method equally applies to visualized flow fields (Schlieren snapshots) and to quantitatively measured flow fields (PIV snapshots).

## 2 Mathematical background and algorithm

The mathematics underlying the extraction of dynamic information from time-resolved snapshots of experimental data is closely related to the idea underlying the Arnoldi algorithm. Starting point of the Arnoldi algorithm is a sequence of vectors (spanning a Krylov subspace  $\mathcal{K}$ ) of the form

$$\{\mathbf{v}, \mathbf{A}\mathbf{v}, \mathbf{A}^2\mathbf{v}, \dots, \mathbf{A}^{n-1}\mathbf{v}\} \quad (1)$$

with  $\mathbf{A}$  as the linear operator (system matrix) that maps a given flow field  $\mathbf{v}$  to a subsequent flow field  $\mathbf{A}\mathbf{v}$  a time-step  $\Delta t$  apart. From this sequence an *orthonormalized* basis  $\mathbf{V}$  is constructed using Gram-Schmidt orthogonalization techniques, and by projection onto this basis  $\mathbf{V}$  according to

$$\mathbf{H} \equiv \mathbf{V}^H \mathbf{A} \mathbf{V} \quad (2)$$

a lower-dimensional matrix  $\mathbf{H}$ , which is of upper Hessenberg form, is obtained. This matrix  $\mathbf{H}$  describes the dynamics of the underlying system (given by  $\mathbf{A}$ ) restricted to the space spanned by the sequence (1). For a sufficiently long sequence that captures the dominant features of the process described by  $\mathbf{A}$  the low-dimensional matrix  $\mathbf{H}$  acts as a proxy of the high-dimensional system matrix  $\mathbf{A}$ ; in particular, the eigenvalues  $\omega$  of  $\mathbf{H}$  approximate some of the eigenvalues of  $\mathbf{A}$  and thus produce stability information (growth rates and phase velocities,  $\omega = \omega_r + i\omega_i$ ) if  $\mathbf{A}$  represents the Jacobian (linearized stability) matrix.

The exact algorithm to construct the orthonormal basis  $\mathbf{V}$  and to extract the Hessenberg matrix  $\mathbf{H}$  relies on the explicit availability of a routine that determines the action of  $\mathbf{A}$  on arbitrary vectors, i.e., given  $\mathbf{q}$  we have to be able to compute  $\mathbf{A}\mathbf{q}$ . This latter requirement for the Arnoldi algorithm is easily satisfied for numerical simulations where the Jacobian matrix  $\mathbf{A}$  is available explicitly or its action is available in form of a subroutine; in experiments, on the other hand, this requirement has to be circumvented, and a successful algorithm has to only rely on data as input. Nevertheless, the general idea of the Arnoldi algorithm can, in spirit, be carried over to the design of an Arnoldi-like algorithm based on snapshots only.

This idea is based on the fact that the action of  $\mathbf{A}$  on a set of column vectors  $\mathbf{V}$  can—for a sufficiently large number of column vectors—be represented by a linear combination  $\mathbf{H}$  of the same set of vectors. In other

words, the vectors are assumed to eventually become linearly dependent. Mathematically, this can be expressed as

$$\mathbf{A}\mathbf{V} = \mathbf{V}\mathbf{H} + \mathbf{r}\mathbf{e}_n^T \quad (3)$$

with  $\mathbf{r}$  as the residual and  $\mathbf{e}_n$  as the  $n$ -th unit vector. We will take advantage of this same idea (the eventual linear dependence of the column vectors) but will apply it to a sequence of snapshots *directly* rather than to an orthonormalized basis.

Taking a set of  $n$  time-resolved (based on the Nyquist criterion) flow field measurements, separated in time by a constant step  $\Delta t$ , and introducing the following notation

$$\mathbf{V}_1^n = \{\mathbf{v}_1, \mathbf{v}_2, \dots, \mathbf{v}_n\} \quad (4)$$

we assume a linear map  $\mathbf{A}$  that maps a given measurement  $\mathbf{v}_j$  onto the subsequent one  $\mathbf{v}_{j+1}$ , that is,  $\mathbf{v}_{j+1} = \mathbf{A}\mathbf{v}_j$ , thus generating a sequence as in (1). For a sufficiently long sequence, we invoke linear dependence of the snapshots and represent the  $n$ -th snapshot by a linear combination of the previous  $n - 1$  snapshots. This is equivalent to the statement (see [19])

$$\mathbf{A}\mathbf{V}_1^{n-1} = \mathbf{V}_2^n = \mathbf{V}_1^{n-1}\mathbf{S} + \mathbf{r}\mathbf{e}_{n-1}^T \quad (5)$$

which is reminiscent of (3), except that the orthonormalized basis  $\mathbf{V}$  in (3) has been replaced by the matrix of measurements  $\mathbf{V}_1^{n-1}$ . Consequently, the upper Hessenberg matrix  $\mathbf{H}$  in (3) is replaced by the matrix  $\mathbf{S}$ . The unknown matrix  $\mathbf{S}$  is determined by minimizing the residual  $\mathbf{r}$  which is equivalent to optimally expressing the  $n$ -th snapshot  $\mathbf{v}_n$  by a linear combination of  $\{\mathbf{v}_1, \dots, \mathbf{v}_{n-1}\}$  in a least-squares sense. From (5) we obtain a least-squares problem for  $\mathbf{S}$  of the form

$$\mathbf{S} = \arg \min_{\mathbf{S}} \|\mathbf{V}_2^n - \mathbf{V}_1^{n-1}\mathbf{S}\| \quad (6)$$

which can easily be solved using a QR-decomposition of  $\mathbf{V}_1^{n-1}$ . Once  $\mathbf{S}$  has been determined, its eigenvalues and eigenvectors can be computed which, in turn, result in the dynamic modes of the underlying snapshot sequence together with their temporal behavior (contained in the eigenvalues of  $\mathbf{S}$ ). The eigenvectors of  $\mathbf{S}$  contain the coefficients of a specific dynamic mode expressed in the snapshot basis  $\mathbf{V}_1^{n-1}$ . The eigenvalues of  $\mathbf{S}$  represent the mapping between subsequent snapshots: unstable eigenvalues are given by a modulus greater than one (i.e., are located outside the unit disk); stable eigenvalues have a modulus less than one (i.e., can be found inside the unit disk). For applications in fluid dynamics, it is common to transform the eigenvalues of  $\mathbf{S}$  using a logarithmic mapping, after which the unstable (stable) eigenvalues have a positive (negative) real part. The procedural steps for computing the dynamic mode decomposition are given in Algorithm 1. Given a sequence of  $n$  snapshots  $\Delta t$  apart in time, two data matrices  $\mathbf{V}_1^{n-1}$  and  $\mathbf{V}_2^n$  are formed that contain the first  $(n - 1)$  snapshots and the same sequence shifted by  $\Delta t$ , respectively. A QR-decomposition of the first sequence is used to solve the linear least square problem (6). The final step consists in computing the eigenvalues and eigenvectors of the matrix  $\mathbf{S}$ , transforming the eigenvalues from the time-stepper format to the format more commonly used in stability theory, and recovering the dynamic modes from weighing the snapshot basis by the eigenvectors of  $\mathbf{S}$ . The analysis of a data sequence, generated by a general nonlinear dynamical system, by a linear snapshot-to-snapshot mapping is linked to Koopman analysis [12, 15] which has recently been extended and applied to fluid mechanical problems, such as direct numerical simulations of a jet in crossflow [18].

The above algorithm is related to other well-known decompositions of flow fields. The matrix  $\mathbf{S}$  can also be obtained from computing the cross-correlation of the data sequences  $\mathbf{V}_1^{n-1}$  and  $\mathbf{V}_2^n$  over one time-step, which is equivalent to solving the above least-squares problem (6) by using the normal equation formulation. In this formulation, a connection to the principal interaction and oscillation patterns, a common technique in atmospheric fluid dynamics (see, e.g., [6, 23]) can be made. In a different but related attempt, a link to the proper orthogonal decomposition can be established, since the correlation between the proper orthogonal modes and their equivalents propagated over one time-step yields a low-dimensional matrix that is unitarily similar to our matrix  $\mathbf{S}$  (see [20] for more details). From this last statement, it should become evident that, contrary to the proper orthogonal decomposition, the dynamic mode decomposition contains not only information about coherent structures, but also about their *temporal evolution*.

Since at no stage of the algorithm the system matrix  $\mathbf{A}$  is needed, various extensions and attractive features of the algorithm should be noted. No specific spatial arrangement of the sampled data is assumed, and the

---

**Algorithm 1** Dynamic mode decomposition
 

---

**Input:** a sequence of  $n$  snapshots  $\{\mathbf{v}_1, \mathbf{v}_2, \dots, \mathbf{v}_n\}$  sampled equispaced in time with  $\Delta t$

**Output:** dynamic mode spectrum  $\lambda_j$  and associated dynamic modes  $\mathbf{DM}_j$  with  $j = 1, \dots, n - 1$

$$\mathbf{V}_1^{n-1} \leftarrow \{\mathbf{v}_1, \mathbf{v}_2, \dots, \mathbf{v}_{n-1}\}$$

$$\mathbf{V}_2^n \leftarrow \{\mathbf{v}_2, \mathbf{v}_3, \dots, \mathbf{v}_n\}$$

$$[\mathbf{Q}, \mathbf{R}] \leftarrow \mathbf{qr}(\mathbf{V}_1^{n-1}, 0)$$

$$\mathbf{S} \leftarrow \mathbf{R}^{-1} \mathbf{Q}^H \mathbf{V}_2^n$$

$$[\mathbf{X}, \mathbf{D}] \leftarrow \mathbf{eig}(\mathbf{S})$$

$$\lambda_j \leftarrow \log(\mathbf{D}_{jj}) / \Delta t$$

$$\mathbf{DM}_j \leftarrow \mathbf{V}_1^{n-1} \mathbf{X}_{(:,j)}$$


---

processing of subdomain data, i.e., data extracted only in a small region of the complete flow domain, as well as the processing of unstructured data is possible. This feature allows to probe a subregion of the flow as to the presence of a specific mechanism. For example, a jet in a crossflow can be analyzed by extracting data from the shear layer atop the counter-rotating vortex pair or by extracting data in the wake of the jet [3, 18]. Either data-set will yield different flow features, time-scales and spatial patterns. We will demonstrate the extraction of flow features from subdomains in the example of an axisymmetric helium jet (see Sect. 3.1). It should also be mentioned that the measurements  $\mathbf{v}_j$  may contain a wide variety of the quantities that describe the dynamics of the flow, for example, velocity fields from PIV-measurements or colormaps from high-speed visualizations. These quantities may even be combined into a composite state vector, such as, e.g., in the simultaneous measurement of fluid velocities by PIV and acoustic radiation by a microphone array in the farfield.

Another attractive feature is the analysis of spatially evolving data. In many applications, the description of a fluid instability in a spatial framework is more appropriate than in a temporal framework. Again, since the system matrix  $\mathbf{A}$  is not formed, but rather extracted from the data set, a simple reorganization of the data sequence in space rather than time will produce a low-dimensional representation of a spatial evolution operator that optimally approximates the mapping of the flow field from one spatial station to the next. The resulting eigenvalues give spatial growth/decay rates and associated spatial frequencies. For further details and examples of subdomain and spatial analysis using the above algorithm the reader is referred to [20].

When processing data sequences by the above DMD-algorithm, a distinction has to be made as to the underlying process. If the snapshots stem from a linear process (for example, a linearized numerical simulations), the dynamic modes extracted from the data sequence coincide with the results of a linear global stability analysis. In this case, the DMD-algorithm (see equation (5)) provides the same results as the classical Arnoldi method (see equation (3)). The DMD-spectrum converges toward the eigenvalues of the linear stability matrix. On the other hand, if the snapshots stem from a nonlinear process, as is the case for most experiments, the dynamic modes represent the coherent invariant structures of the best *linear* map from one snapshot to the next. For sufficiently long data sequences, only neutrally stable structures should be found, since instabilities will have saturated and stable (decaying) structures will have vanished. In this case, the DMD will detect the dominant frequencies and associated spatial structures in the flow and separate the relevant from the irrelevant flow features. When compared with proper orthogonal decomposition, we can state that POD modes enforce *spatial orthogonality* (decorrelated structures) while keeping multiple frequencies in the evolution of each individual POD mode, whereas DMD modes are *temporally orthogonal* (pure frequencies) but show, in general, spatial non-orthogonality. For experimental data from a saturated nonlinear process, the extraction of pertinent frequency information and its associated structures may be more critical than an energy ranking of spatially decorrelated structures. For shorter data sequences, or transient fluid processes, stable and unstable structures can be identified, and the interpretation of their relevance has to be performed more carefully; the content of a particular structure (together with its temporal behavior) in the original data sequence can aid in the distinction of dynamically important and noisy flow features. Along this line, it should be mentioned that the dynamic mode decomposition is a robust tool to identify prevalent frequencies and coherent structures, even in the presence of experimental uncertainties, measurement errors or environmental noise.

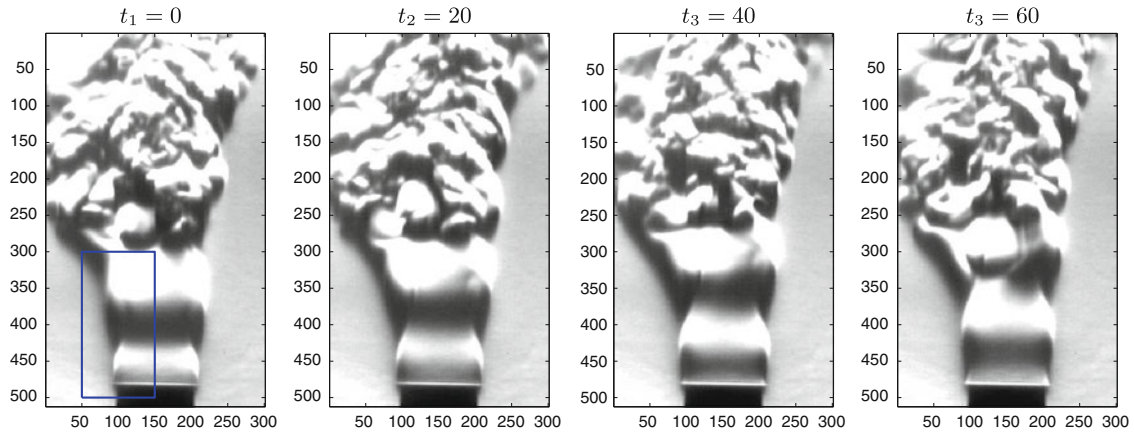


**Fig. 1** A selection of Schlieren snapshots of a low-density helium jet with a density ratio of  $S = 0.14$  and a Reynolds number of  $Re = 940$ . The window for which time-resolved data is extracted is indicated in the leftmost snapshot  $u$

### 3 Applications

We will demonstrate the dynamic mode decomposition technique on two examples. These examples have been chosen to represent experimental data of various degrees of informational content. The first example, a helium jet, uses Schlieren techniques to visualize the dynamics of the fluid structure; thus, only a scalar field—proportional to the density gradient and quantified by its location on a grey-scale colormap—is being processed. The second example, a forced and unforced axisymmetric jet, will process fully time-resolved PIV-data; in this case, complete velocity information of the flow field is available for the decomposition.

#### 3.1 Dynamic mode decomposition of a helium jet

The first example concerns a low-density helium jet exhibiting a global instability. The jet has been produced using a contoured nozzle of diameter  $D = 19$  mm directed vertically upwards and injected into quiescent air at temperature  $T = 20^\circ\text{C}$  and pressure  $p = 1$  atm. High-speed videos of the flow have been captured using a PHANTOM V4.2 CMOS camera combined with a Z-type Schlieren setup (based on a 5 mm dia. white LED light source) which used a horizontal knife-edge to properly resolve vertical density gradients. The flow has been sampled at a framerate of 1,600 frames per second with a  $580\ \mu\text{s}$  exposure time and a spatial resolution of  $512 \times 512$  pixels. A typical sequence of the jet for a density ratio  $S = \rho_{\text{jet}}/\rho_{\text{amb}} = 0.14$  and a Reynolds number of  $Re = 940$  (based on the jet velocity and the nozzle diameter) is shown in Fig. 1 where the first snapshot (Fig. 1a) also contains the size and location of our interrogation window for the subsequent DMD-analysis. At these parameter settings the axisymmetric jet is characterized by a pocket of absolute instability near the nozzle exit (see [16]) which manifests itself in a self-sustained, axisymmetric, oscillatory behavior of the jet.

The visualized density gradients have been mapped onto a grey-scale colormap and parameterized as to their location on this map. A sequence of frames then constitutes a quantified scalar field proportional to the density gradient which can then be processed by the dynamic mode decomposition. Taking advantage of the fact that the decomposition can equally be applied to the full flow field or a smaller interrogation window, we invoke the symmetry of the flow and extract data from a subdomain indicated in Fig. 1a. In addition, it is important to mention that the projection of an axisymmetric density profile onto a two-dimensional colormap plane does not influence the temporal dynamics that will be extracted from the data-sequence by the dynamic mode decomposition.

The reshaped snapshots form a vector basis in which the dynamics of the flow, i.e., the mapping from one image to the next, is approximated. This mapping which is, in general, a  $N \times N$  matrix  $\mathbf{A}$  with  $N$  as the total number of pixels in each image is then projected onto the vector basis  $\mathbf{V}_1^{n-1}$  to yield a lower-dimensional  $(n-1) \times (n-1)$  system matrix  $\mathbf{S}$  (with  $n$  as the number of processed snapshots; in our case  $n = 100$ ) governing the coefficients of a linear expansion in the vector basis. In particular, the eigenvalues of  $\mathbf{S}$  will approximate some of the eigenvalues of  $\mathbf{A}$ .



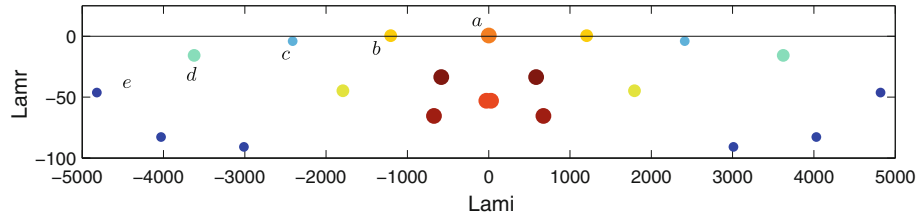


**Fig. 2** DMD-spectrum of a helium jet for density ratio  $S = 0.14$  and Reynolds number  $Re = 940$ . The marker size indicate the spatial coherence of the associated dynamic modes (see text; larger symbols: large-scale structures; smaller symbols: small-scale structures)

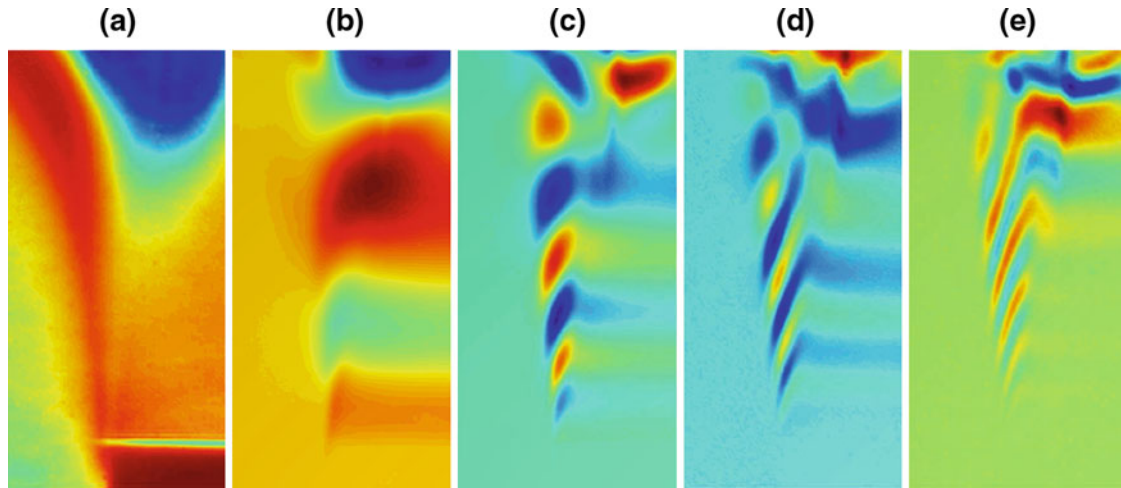
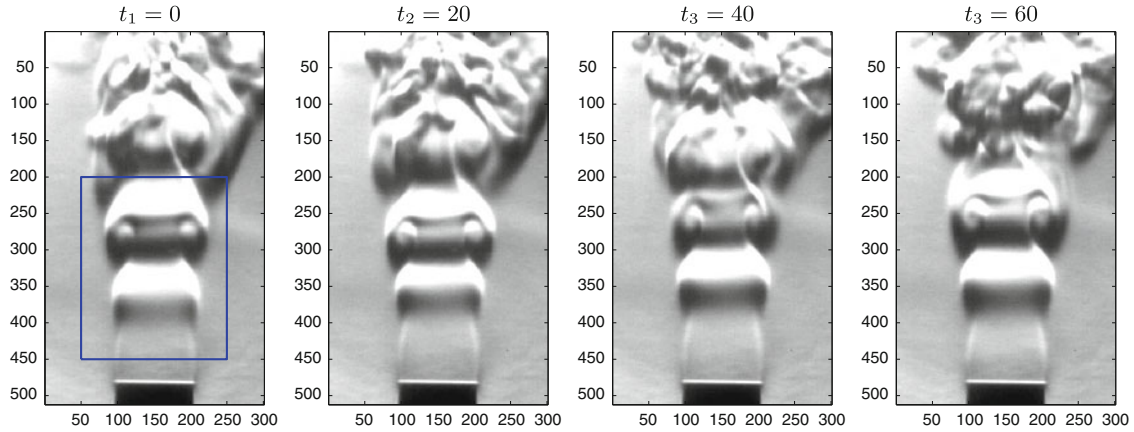


**Fig. 3** Five representative dynamic modes (real part only) associated with the spectrum in Figure 2

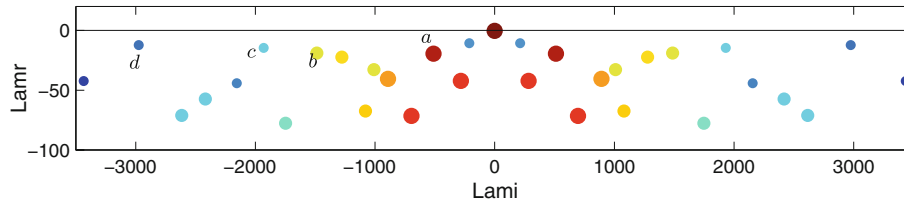
The spectrum extracted from the above sequence of snapshots is displayed in Fig. 2. It shows qualities of a typical spectrum for an advection-diffusion dominated flow. The eigenvalues show a strong alignment along the horizontal neutral line, but are overall damped. An eigenvalue at the origin (labelled  $a$ ) is present which represents the steady state; its corresponding eigenvector displays the mean flow field. This feature is also present in a POD analysis of the same flow field: the first, most dominant, right singular vector of the snapshot basis consists of the mean flow (see [2]). The least stable modes then fall on parabolic arcs, denoted by  $b$  through  $e$  in Fig. 2. Since over the temporal observation period the flow is in an equilibrated state, we do not expect and observe any unstable eigenvalue. For even longer observation periods and data sequences, the damping rates of the dominant dynamic modes will approach the neutral line. The color coding and symbol size of the eigenvalues represent a measure of coherence of the associated modes (similar to the energy content of POD modes) and help in the separation of relevant structures from noise-contaminated ones. This coherence measure is computed by projecting individual dynamic modes onto energy-ranked proper orthogonal modes (except the mean flow); the resulting coefficients of this projection give a ratio of large-scale to fine-scale structures. This feature adds information about spatial coherence and scales to the temporal information contained in the spectrum.

Figure 3 presents five dynamic modes associated with the labeled eigenvalues in Fig. 2. As mentioned before the mode corresponding to label  $a$  represents the mean flow, while the higher modes  $b$  through  $e$  increasingly show the presence of small-scale (but coherent) structures. The support of the dynamic modes is clearly located at the diverging outer edge of the jet where vortex roll-up, mixing and entrainment processes are prevalent.

A characteristic slanted pattern of the oscillatory and slightly damped dynamic modes is clearly visible and conforms to findings from numerical stability analyses of linearized flows (Nichols, J.W.: Private communication, 2008) [7]. Only the real part of the dynamic modes has been shown in Fig. 3; the corresponding imaginary part is phase-shifted by  $90^\circ$  which, when multiplied by the corresponding temporal dynamics (contained in the eigenvalue), produces an advective-diffusive process for each individual dynamic mode structure.



**Fig. 4** A selection of Schlieren snapshots of a low-density helium jet with a density ratio of  $S = 0.5$  and a Reynolds number of  $Re = 1850$ . The window for which time-resolved data is extracted is indicated in the leftmost snapshot A u



**Fig. 5** DMD-spectrum of a helium jet for density ratio  $S = 0.5$  and Reynolds number  $Re = 1850$ . For an explanation of the symbol size the reader is referred to the text

A second case is concerned with a different parameter regime. The density ratio  $S = \rho_{\text{jet}}/\rho_{\text{amb}}$  has been substantially increased to  $S = 0.5$  and a Reynolds number of  $Re = 1,850$  has been chosen. At these parameter settings, a primary axisymmetric absolute instability is still present, but somewhat weaker. Again, we first inspect a selection of snapshots (see Fig. 4) to conclude that a more pronounced vortex roll-up stage and a less rapid breakdown into turbulent fluid motion can be observed. These features should also be reflected in the shape of the DMD-spectrum as well as in the shape of the dynamic modes. As before we will not concentrate our analysis on the entire flow domain but rather extract data from a smaller window as indicated in Fig. 4a; as before,  $n = 100$  snapshots from this subdomain will be processed.

The spectrum extracted from the data via the low-dimensional system matrix  $\mathbf{S}$  is presented in Fig. 5. It is again dominated by elements reminiscent of an advection-diffusion spectrum. In contrast to the previous case, though, more arc-like eigenvalue clusters are visible, a feature that is often observed in the numerical calculation of global spectra. Structures within such an eigenvalue arc contain fluid elements that show similar support in the flow domain but are characterized by different local wavenumbers (see, e.g., [4]). In superposition, they often form traveling coherent structures or wavepackets.

Four selected dynamic modes have been extracted by concentrating on small damping rates and spatial coherence. This choice is motivated by the assumption that within the sampling period the corresponding structures were persistent, observable, and representative of the large-scale features of the flow. Nevertheless, the possibility of a full analysis by superposing coherent structures weighted by their extracted exponential behavior should be considered. The mode corresponding to the eigenvalue at the origin again captures the mean flow and is omitted this time. The sequence of dynamic modes presented in Fig. 6 illustrates a dominant scaling between the local scale of the flow feature and its temporal frequency, suggesting that the dynamic mode decomposition has succeeded in extracting a valid (though approximate) dispersion relation from the experimental data. The support of the modes is clearly concentrated near the edge of the mixing layer which becomes more evident as the scales becomes smaller; this is a consequence of the prevalence of density gradients near the edge of the helium jet.

Slanted structures are again observed, and the appearance of small-scale structures (linked to the breakdown of the jet) is more prevalent further downstream of the jet nozzle. This is in accordance with observation and physical intuition.

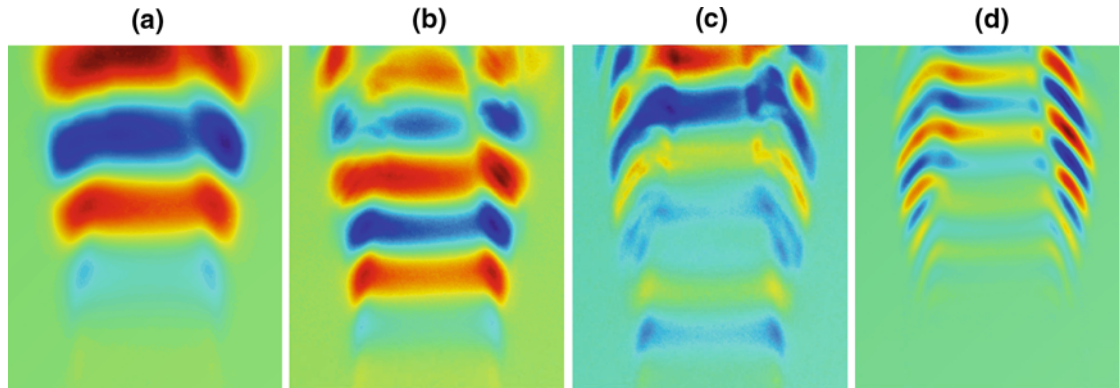


**Fig. 6** Four representative dynamic modes (real part only) associated with the spectrum in Fig. 5

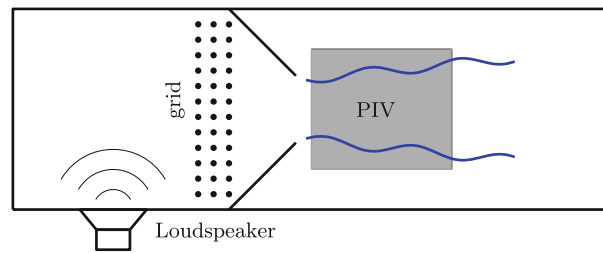


**Fig. 7** Sketch of the experimental setup for the forced/unforced axisymmetric jet

### 3.2 Response of an axisymmetric jet to external forcing

Whereas the previous example demonstrated the possibility of extracting coherent dynamic behavior from a sequence of snapshots that visualize (by a pixelized colormap proxy) the flow dynamics, the next example will be based on fully time-resolved measurements of the fluid velocities by particle-image velocimetry (PIV). This type of measurements is significantly more advanced and involved and yields detailed information about the flow dynamics that rivals numerical simulations of the same flow configuration.

A sketch of the experimental setup is shown in Fig. 7. A jet emanates from a plenum by passing through a screen followed by a conical contraction. A loudspeaker inside the plenum is used to impose a time-harmonic acoustic signal on the jet. A quadratic interrogation area for the time-resolved PIV measurements is located 10 mm downstream of the nozzle exit and measures 54.7 mm in the streamwise and normal coordinate direction. The fluid is seeded with PIV tracer particles (oil droplets 2–3  $\mu\text{m}$  in size), and the interrogation window is resolved by a  $63 \times 63$  grid. Individual snapshots are separated by 0.333 ms which results in a Nyquist frequency of 1,500 Hz, well above the characteristic frequency given by the jet velocity and jet diameter. The jet diameter is 30 mm and the center velocity of the jet is 7.5 m/s, yielding a Reynolds number based on these quantities of  $Re = 14,767$ . Once a time-resolved snapshot sequence is available, it can be processed by the DMD-algorithm to reduce the full dynamics captured in the snapshots down to a lower-dimensional set that reproduces the original data in an optimal manner. Both velocity components will be taken into account, even though a single component would suffice to determine the dynamic characteristics. Each snapshot thus consists of  $2 \times 63 \times 63 = 7938$  elements; a total of  $n = 101$  snapshots have been processed. Furthermore, two cases will be considered and contrasted: the dynamics of an axisymmetric jet evolving naturally, and the dynamics of the same jet under harmonic external excitation of a given frequency.

To an observer the snapshot sequence of the forced and unforced jet differ only slightly which makes the detection of the response behavior of the jet to external excitation rather difficult. An analysis based on the proper orthogonal decomposition (POD) also has difficulties in establishing a clear difference between the two cases: spatial changes in the modal shapes are detectable, but a characterization of the changed temporal response dynamics is difficult. It is possible to extract a scalar signal from the jet and Fourier-transform the signal which should show the presence of a frequency response to an externally imposed forcing. This procedure, however, cannot identify a spatial structure that corresponds to the response. On the other hand, the spectrum obtained from the dynamic mode decomposition uncovers a marked difference between the two



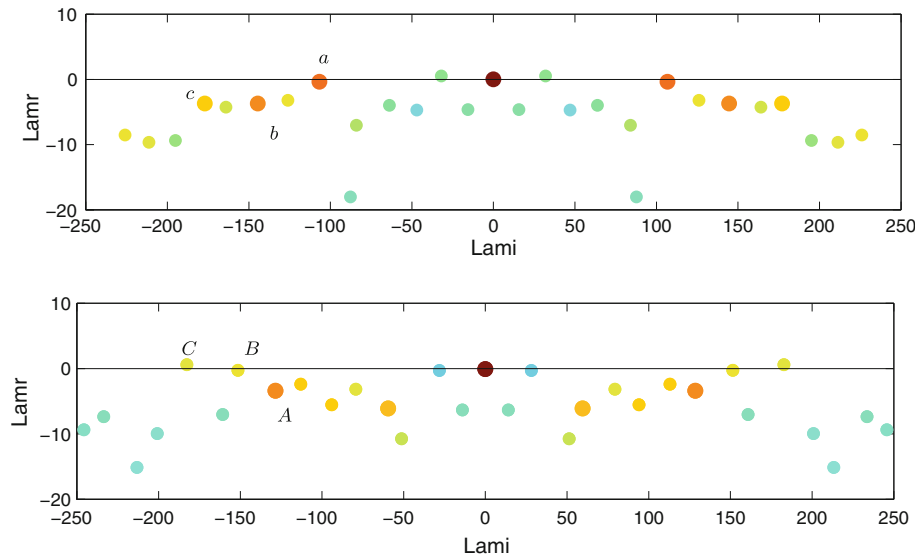


**Fig. 8** DMD-spectrum of an unforced (*top*) and harmonically forced (*bottom*) axisymmetric jet

cases (see Fig. 8); the corresponding dominant dynamic modes illustrate the associated spatial structures (see Figs. 9 and 10).

The unforced spectrum shows a coherent structure with negligible damping at a frequency of approximately  $\lambda_i/2\pi = 110$  Hz (label (a) in Fig. 8), equivalent to a Strouhal number of 0.44; this value falls within the range of ‘preferred’ Strouhal numbers given in [10]. Higher harmonics are not present in a significant way. The situation is markedly different for the spectrum of the forced jet. In this case, the natural frequency can no longer be detected by the dynamic mode decomposition. In its place, the frequency of the forcing ( $f_f = 150$  Hz) and a higher combination frequency can be observed (label (B) and (C) in Fig. 8). It appears that for the experimental parameters, the jet rather easily adopts the frequency of the forcing, showing an appreciable amount of receptivity to harmonic external forcing. In this sense, the jet behaves as a noise amplifier rather than a self-sustained oscillator [9].

Whereas the response behavior of the axisymmetric jet to harmonic forcing could have been quantified by a Fourier-analysis, additional information can be gained from the dynamic mode decomposition by examining the change in the structures associated with the above-mentioned eigenvalues. This is shown in Figs. 9 and 10, respectively. For the unforced case, medium-scale structures located at the edge of the mixing layer can be observed. These structures are mainly responsible for the roll-up of the outer shear layer and the entrainment of quiescent fluid into the jet. The size and structure of these fluid elements can be used to compute a first estimate of the amount of mixing. It is also noticeable that the vortical structures tend to become larger-scale as we move downstream; rather little dynamic features are observed near the nozzle (left side of the PIV interrogation window). The forced case shows distinct differences: in this case, large-scale structures dominate the mixing/entrainment process further upstream than in the unforced case (compare Figs. 9b and 10b) and are expected to significantly change the roll-up of the outer shear layers. From this analysis it can be concluded that the primary effect of forcing is concentrated near the nozzle exit where oscillatory vortical fluid elements (eigenvalue (B) in Fig. 8 and associated mode in Fig. 10b) are introduced that dominate the forced dynamics. For the unforced jet, the decomposition shows a more typical behavior characterized by the progressive roll-up of the outer shear layer in the downstream direction.

#### 4 Summary and conclusions

The extraction of global flow features from a sequence of experimental data has been attempted by computing a low-dimensional representation of the flow dynamics directly from the experimental data without recourse to an underlying model. This purely data-based decomposition method produces global modes, if the sequence has been generated by a linearized evolution equation (in the case of numerical simulations), or dynamic modes, if the sequence stems from measurements taken from physical experiments. The data-based nature of

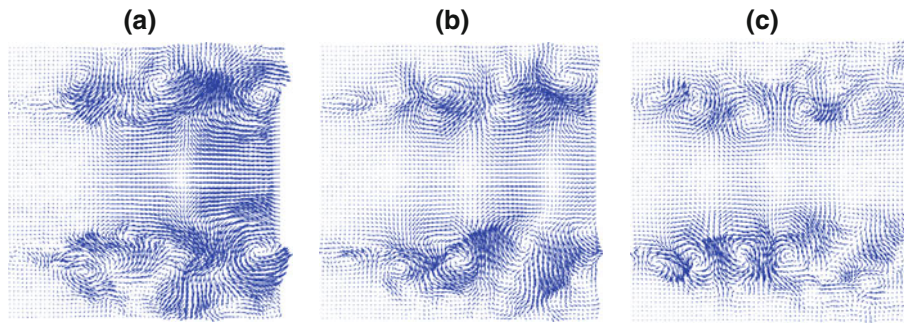


**Fig. 9** Selected dynamic modes of an unforced axisymmetric jet. The modes correspond to the labels in Fig. 8(a)

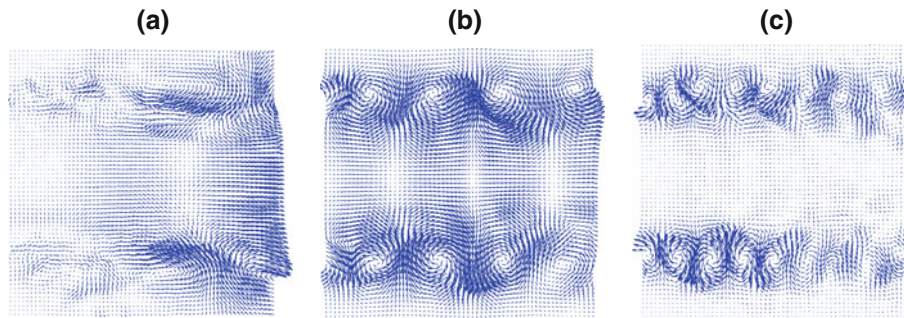


**Fig. 10** Selected dynamic modes of a harmonically forced axisymmetric jet. The modes correspond to the labels in Fig. 8(b)

the algorithm allows the focus on specific regions of the flow where interesting and relevant dynamic processes take place and the dissection of complex fluid phenomena into localized dominant features. The method allows both temporal and spatial analyses; in this article, only results from a temporal analysis have been presented.

In the case of visualizations by a passive scalar field, the results from Schlieren pictures of a low-density helium jet have shown typical modal structures on the shear layer of the jet that exhibit the commonly known scaling of temporal frequencies and spatial wavenumbers of the associated modal structure.

When time-resolved PIV-data have been used, the dynamic mode decomposition could clearly distinguish between the flow fields of a forced and unforced axisymmetric jet. This difference was reflected in the temporal spectrum as well as in the spatial structure of the associated least damped dynamic modes.

This type of decomposition technique is hoped to provide a valuable tool in the experimentalist's arsenal to express the dominant behavior of the flow under investigation in terms of a few coherent structures and their temporal (and/or spatial) characteristics. It is equally hoped that this type of decomposition will help in providing more insight into the key physical mechanisms of a variety of flows that are studied by experimental (or even numerical) means.

**Acknowledgments** Support of the first author from the Agence Nationale de la Recherche (ANR) through the “chaires d'excellence” program and the Alexander-von-Humboldt Foundation is gratefully acknowledged. The first author thanks Christoph Mack for helpful comments on an earlier draft.

## References

1. Antonia, R.A.: Conditional sampling in turbulence measurement. *Ann. Rev. Fluid Mech.* **13**, 131–156 (1981)
2. Aubry, N.: On the hidden beauty of the proper orthogonal decomposition. *Theor. Comput. Fluid Dyn.* **2**, 339–352 (1991)
3. Bagheri, S., Schlatter, P., Schmid, P.J., Henningson, D.S.: Global stability of a jet in crossflow. *J. Fluid Mech.* **624**, 33–44 (2009)
4. Barbagallo, A., Sipp, D., Schmid, P.J.: Closed-loop control of an open cavity flow using reduced-order models. *J. Fluid Mech.* **641**, 1–50 (2009)
5. Edwards, W.S., Tuckerman, L.S., Friesner, R.A., Sorensen, D.C.: Krylov methods for the incompressible Navier–Stokes equations. *J. Comput. Phys.* **110**, 82–102 (1994)
6. Hasselmann, K.: POPs and PIPs. The reduction of complex dynamical systems using principal oscillations and interaction patterns. *J. Geophys. Res.* **93**, 10975–10988 (1988)

7. Heaton, C.S., Nichols, J.W., Schmid, P.J.: Global linear stability of the non-parallel Batchelor vortex. *J. Fluid Mech.* **629**, 139–160 (2009)
8. Herzog, S.: The large scale structure in the near-wall region of turbulent pipe flow. Ph.D. Dissertation, Department of Mechanical Engineering, Cornell University, Ithaca, NY (1986)
9. Huerre, P., Monkewitz, P.A.: Local and global instabilities in spatially developing flows. *Ann. Rev. Fluid Mech.* **22**, 473–537 (1990)
10. Hussain, A.K.M.F., Zaman, K.B.M.Q.: The ‘preferred mode’ of the axisymmetric jet. *J. Fluid Mech.* **110**, 39–71 (1981)
11. Hussain, A.K.M.F.: Coherent structures and turbulence. *J. Fluid Mech.* **173**, 303–356 (1986)
12. Lasota, A., Mackey, M.C.: *Chaos, Fractals and Noise: Stochastic Aspects of Dynamics*. Springer Verlag, Berlin (1994)
13. Lehoucq, R.B., Scott, J.A.: Implicitly restarted Arnoldi methods and subspace iterations. *SIAM J. Matrix Anal. Appl.* **23**, 551–562 (1997)
14. Lumley, J.L.: *Stochastic Tools in Turbulence*. Academic Press, New York (1970)
15. Mezić, I.: Spectral properties of dynamical systems, model reduction and decompositions. *Nonlinear Dyn.* **41**, 309–325 (2005)
16. Monkewitz, P.A., Sohn, K.D.: Absolute instabilities in hot jets. *AIAA J.* **26**, 911–916 (1988)
17. Rajagopalan, S., Antonia, R.A.: Use of a quadrant analysis technique to identify coherent structures in a turbulent boundary layer. *Phys. Fluids* **25**, 949–956 (1982)
18. Rowley, C.W., Mezić, I., Bagheri, S., Schlatter, S., Henningson, D.S.: Spectral analysis of nonlinear flows. *J. Fluid Mech.* **641**, 115–127 (2009)
19. Ruhe, A.: Rational Krylov sequence methods for eigenvalue computations. *Linear Algebra Appl.* **58**, 279–316 (1984)
20. Schmid, P.J.: Dynamic mode decomposition of numerical and experimental data. *J. Fluid Mech.* **656**, 5–28 (2010)
21. Schoppa, W., Hussain, A.K.M.F.: Coherent structure dynamics in near wall turbulence. *Fluid Dyn. Res.* **26**(2), 119–139 (2000)
22. Theofilis, V.: Advances in global linear instability analysis of nonparallel and three-dimensional flows. *Prog. Aerosp. Sci.* **39**, 249–315 (2003)
23. von Storch, H., Bürger, G., Schnur, R., von Storch, J.: Principal oscillation patterns: a review. *J. Clim.* **8**, 377–400 (1995)